

Received November 15, 2020, accepted November 25, 2020, date of publication December 2, 2020, date of current version December 17, 2020.

Digital Object Identifier 10.1109/ACCESS.2020.3041855

# An Innovative Control Allocation Framework for a Novel Tiltrotor Aircraft

YIFAN XU<sup>1</sup>, QIAN ZHANG<sup>2,3</sup>, AND ZELONG YU<sup>1</sup>

<sup>1</sup>School of Instrumentation Science and Opto-electronics Engineering, Beihang University, Beijing 100191, China

<sup>2</sup>School of Aeronautic Science and Engineering, Beihang University, Beijing 100191, China

<sup>3</sup>Hefei Innovation Research Institute, Beihang University, Hefei 230012, China

Corresponding author: Qian Zhang (victoryqian175@163.com)


**ABSTRACT** Control allocation is still a challenge for tiltrotor aircraft due to effectors' redundancy, dramatic nonlinearities and cross-coupling. Besides this, the external disturbance caused by the unique configuration of tiltrotor such as larger wing area and tiltable mechanism puts forward extra security requirement on control allocation method. Thus, this paper proposes an innovative control allocation framework from the perspective of flight safety to address this problem. Firstly, an effector distribution management scheme based on remaining control ability index (RCAI) is developed to reduce the effector saturation and ensure flight safety. Secondly, the energy consumption models for two classes of effectors: thrust vectoring and aerodynamic surfaces are introduced respectively for the subsequent optimization problem mathematically. Then, the null space transition is used to find the minimum-energy control input of effectors. Finally, key parameters of energy consumption model are identified by experiments. The real-time hardware-in-loop simulation platform is adopted to demonstrate the effectiveness of the proposed control allocation framework. Experimental results show that the energy consumption of proposed method can reduce by about 63.5% comparing to traditional control allocation method.

**INDEX TERMS** Novel tiltrotor aircraft, effector distribution management scheme, flight safety, energy consumption model, minimum-energy control allocation.

## I. INTRODUCTION

During recent years, tiltrotor aircraft has gained remarkable attention on aviation industry [1]–[4] due to the broad flight envelope: from hover state, typical of rotorcraft, to high cruising-speed characteristic of fixed-wing aircraft. However, the unique structural characteristics, such as larger wing area and tiltable mechanism, make it a strong nonlinear and coupling system [5], [6]. Besides this, the number of control effectors and their dramatically change effectiveness with different flight states are great challenges for tiltrotor aircraft. According to [7]–[9], the best option to solve this problem is to design a control allocation framework that distributes the virtual moment commands to the redundant effectors.

Many control allocation methods have been proposed to solve the problem of redundantly-actuated unmanned aerial vehicles (UAVs). Reference [10] proposes a control allocator for a fully-actuated tilting quadrotor platform to decouple the platform's rotation and translation by mapping

The associate editor coordinating the review of this manuscript and approving it for publication was Nasim Ullah .

the attitude and position commands to the unique actuator. In [11], a control allocation strategy based on genetic algorithms is designed to find the optimal actuator's solution. The method is validated in two simulation scenarios of a redundantly-actuated planar robot and a generalized hexa-rotor. For a generically tilted multirotor, [12] proposes a decoupling method between the total force and total moment by the definition of some algebraic conditions on the control allocation matrices. For a hexacopter with tiltable rotors, [13] transforms the nonlinear allocation problem into a linear problem through variable transformation, then Moore–Penrose pseudoinverse is used to get the minimum norm solution.

An actuator-dynamics-based dynamic control allocation [14] scheme is developed for flight control of a small fixed-wing UAV. Stability analysis and high-fidelity simulations both demonstrate the effectiveness of the proposed method. Weighted Pseudo-Inverse [15], Redistributed Pseudo-Inverse [16] and Cascading Generalized Inverse [17] have also been proposed to address allocation problem for fixed-wing.

Differing from the typical tilting multirotor and fixed-wing aircraft, tiltrotor aircraft usually possess two class of effectors: the only control effectors in hover are thrust vectoring, whereas classical aerodynamic surfaces are used in forward flight. Thus, some researchers [18]–[20] propose a weight allocation method which is concerned with air-speed or rotor-tilt angle of tiltrotor. The open source flight control system PixHawk [21] also adopts this control concept to control the tiltrotor aircraft. A control allocation method based on the channel throttles and trim calculations is proposed for the hover state of tiltrotor in [22]. Due to limited onboard computational power, [23] designs a daisy-chaining approach to handle allocation of redundant actuators for a tiltwing UAV, which gives a defined order of priority among redundant actuators. Reference [24] also adopts a daisy-chaining logic to manage effector redundancy for a tiltrotor according to the actuator availability and effectiveness. A prioritized control allocation in [25], which aims to prevent control saturation, is proposed for a quad tiltrotor. Reference [26] designs a series-parallel control allocation method combined by choosing the appropriate bandwidth in the frequency domain for all-state flight of a tri-tiltrotor. Paper [27] proposes a control allocation method based on null space to solve path dependency problem caused by the incremental controllers. Flight tests were performed to verify the effectiveness of the proposed method.

Common control allocation algorithms focus on three principal approaches: Direct Allocation (DA) [28], Generalized Inverse (GI) [29] and Mathematical Programming (MP) [30] or their variants. Apart from the above methods, some advanced algorithms such as additional dynamic augmentation [31], and input matrix factorization [32] have also been used in control allocation. However, limited by the computing capability, the DA and MP methods are difficult to run in real time for the digital flight control system whose control frequency is up to 200-400 Hz. Traditional GI method and its variant are not suitable for solving the allocation problem of tiltrotor aircraft which may yield the potential suboptimal result due to position and rate limits of the effectors.

The advantage of redundancy effectors not only allows to optimize some objectives such as minimum energy or drag, but also provides the possibility of improving flight safety. Most research work such as [33]–[35] focus on fault tolerant control after actuator faults happened, which not exploits the potentiality of redundancy effectors before the failure of actuators. The larger wing area and tiltable mechanism of tiltrotor will bring more external disturbance and model uncertainty, which put forward higher security requirement on control. However, it seems that few literatures take flight safety into consideration during the design process of control allocation. From the analysis of effectors' control effectiveness, we have found that the proper selection of switch point between the thrust vectoring and aerodynamic surfaces (the time of aerodynamic surfaces participating in control and the time of thrust vectoring exiting control) can effectively guarantee the control ability of tiltrotor, thus leading to

certain anti-interference ability and ensure flight safety. Thus, we introduce the remaining control ability index (RCAI) is utilized to determine these switch points and an effector distribution management scheme (EDMS) based on RCAI is developed. Besides this, the primary target of control allocation is that the commanded three-axis moment should be produced exactly by the effectors' action. On the basis of realizing commanded moment, secondary objectives such as minimum energy can be achieved due to redundancy. Considering that the energy efficiency of thrust vectoring and aerodynamic surfaces are quite different, we further study the energy consumption model for two class of effectors. Then, the energy optimized method based null space transition [36], [37] is developed due to its low computational complexity.

Therefore, we develop an innovative control allocation framework from the perspective of flight safety to distribute the virtual moment commands for tiltrotor. The main contributions of this work can be summarized as follows:

(1) The RCAI is utilized to determine the switch point between the thrust vectoring and aerodynamic surfaces based on the analysis of effectors' control effectiveness. An EDMS based on RCAI is developed to select the proper effector combinations according to flight state and ensure flight safety.

(2) The energy modeling methods for two classes of effectors: thrust vectoring and aerodynamic surfaces are studied. Ground tests and real flight data are utilized to determine key model parameters.

(3) Control allocation method based on null space transition is proposed to find minimum-energy control input of effectors by using the energy consumption model.

The paper is organized as follows: the tiltrotor aircraft configuration and the control allocation problem are formulated in Section II. Section III introduces the EDMS, which is based on RCAI. We discuss the energy modeling methods for two classes of effectors and the minimum-energy control allocation method based on null space transition is presented Section IV. Followed by conclusion in Section V.

## II. PROBLEM FORMULATION

### A. TILTROTOR AIRCRAFT CONFIGURATION

The 3-D model of the novel tiltrotor and corresponding control effectors are presented in Figure 1. The coordinate systems are defined as follows:  $O_b - X_b Y_b Z_b$  is the body frame. Where  $O_b$  is at the center of gravity,  $X_b$  pointing to the front of the tiltrotor,  $Y_b$  pointing right and  $Z_b$  pointing down.  $O_n - X_n Y_n Z_n$  is the navigation frame which coincides with the geographic frame (north, east and down). For the reader's convenience, Table 1 summarizes all the main symbols used in the paper.

The novel tiltrotor has three flight phases: vertical takeoff and landing (VTOL), transition and level flight. Differing from traditional UAVs, this aircraft adopts flying wing configuration, which improves the lift-drag ratio. Besides this, normal horizontal tail, elevator and rudder are cancelled, which also increases the difficulty of control.

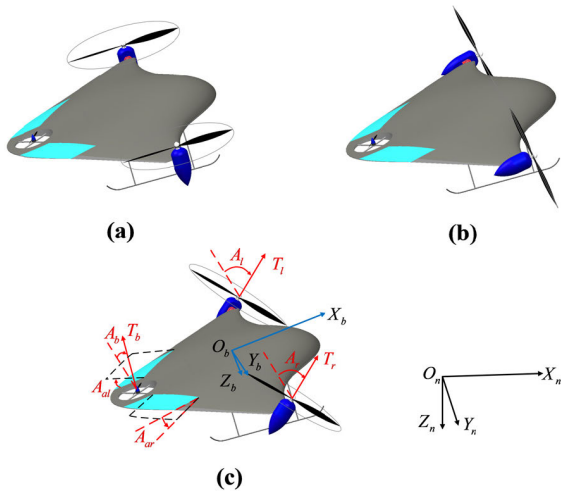


FIGURE 1. 3-D model and three flight phase of the novel tiltrotor. (a) VTOL phase. (b) Level phase. (c) Transition phase.

TABLE 1. Main symbols used in the paper.

Definition	Symbol
Local linear effectiveness matrix	$B_{local}$
Thrust synchronous component	$T_m$
Thrust differential component	$T_n$
Deflection angle of elevator	$A_e$
Deflection angle of aileron	$A_d$
Roll, pitch and yaw angular rate	$p, q, r$
Dynamic pressure	$Q$
Air density	$\rho$
Sideslip angle	$\beta$
Attack angle	$\alpha$
Remaining control ability index	$\rho(M_{des}, \xi)$
Effector input from pseudo-inverse module	$u_0$
Effector input from control decoupling module	$u_{cor}$
Effector input from energy-optimized	$u_e$
Thrust efficiency	$\eta_m$
Deflection angle efficiency	$\eta_w$

As seen in Figure 1(c), the aircraft features eight effectors in all. The two main rotor at both ends of the wings can tilt with  $Y_b$  from  $-10^\circ$  to  $90^\circ$  ( $0^\circ$  tilt angle means VTOL phase, and  $90^\circ$  tilt angle means level flight phase). The ducted fan, which equipped at the end of vehicle can swing with  $X_b$  from  $-45^\circ$  to  $45^\circ$  to provide both the pitch and yaw moment during hover and transition flight. Combining the functions of an elevator and an aileron, the two elevons are used to provide aerodynamic moment in transition and level flight, which can swing up and down from  $-20^\circ$  to  $20^\circ$ . The whole effectors can be divided into two classes: thrust vectoring and aerodynamic surfaces. These effectors are summarized in Table 2.

During VTOL phase, two main rotors in vertical state are the main lift source for hover flight. The two elevons provide

TABLE 2. List of control effectors.

	Symbol	Control Effectors
Thrust vectoring	$T_r$	Thrust of right rotor
	$T_l$	Thrust of left rotor
	$T_b$	Thrust of ducted fan
	$A_b$	Deflection angle of ducted fan
	$A_r$	Deflection angle of right rotor
Aerodynamic surfaces	$A_l$	Deflection angle of left rotor
	$A_{or}$	Deflection angle of right elevon
	$A_{ol}$	Deflection angle of left elevon

trivial moment due to low dynamic pressure, while a ducted fan is designed to produce pitch and yaw moment. In level flight phase, gravity is mainly countered by aerodynamic forces. The two rotors are tilted to  $90^\circ$  and provide thrust to overcome aerodynamic drag in level flight. The ducted fan is inactive to reduce additional energy consumption, while two elevons are utilized to generate roll and pitch moment. During transition phase, the tiltrotor is controlled by all control effectors with the increase of aerodynamic effects. It should be noted that the nonlinearities and cross-coupling of effectors' effectiveness introduced by tilt mechanism and airspeed lead to challenges during transition phase, thus we will discuss reasonable arrangement between the thrust vectoring and aerodynamic surfaces in detail in section III from flight safety point of view.

### B. THREE-AXIS MOMENT DEMANDS

The general relationship between pseudo-controls  $v$ , states  $x$  and effectors  $u$  can be described as:

$$v = h(x, u) \tag{1}$$

where  $v \in R^{3 \times 1}$  is the desired three-axis moment,  $u \in R^{n \times 1}$  denotes the nth effectors input. For different flight operating point  $[x_0, u_0]$ , the local linear effectiveness matrix  $B_{local} \in R^{3 \times n}$  is defined as:

$$B_{local} = \left. \frac{\partial v}{\partial u} \right|_{x_0, u_0} = \left. \frac{\partial h(x, u)}{\partial u} \right|_{x_0, u_0} \tag{2}$$

Thus, the relationship between pseudo-controls  $v$  and effectors  $u$  can be approximated linearly as:

$$v = B_{local}u \tag{3}$$

### C. POSITION AND RATE LIMITS ON THE EFFECTORS

For an actual flight, the effectors are limited by the physical constraints: position and rate saturation. Both the position and rate constraints of effectors input  $u = [u_1, u_2 \dots u_n]^T$  can be expressed as:

$$\{u_i | \underline{U}_i \leq u_i \leq \bar{U}_i\}, \quad i = 1, 2 \dots n \tag{4}$$

where  $\underline{U}_i$  and  $\bar{U}_i$  denote the lower and upper bound for  $i$ th effector respectively, which are given as follows:

$$\begin{cases} \underline{U}_i = \max \{ \underline{u}_i, u_i^{pre} + \dot{\underline{u}}_i \cdot \Delta t \} \\ \bar{U}_i = \min \{ \bar{u}_i, u_i^{pre} + \dot{\bar{u}}_i \cdot \Delta t \}, \end{cases} \quad i = 1, 2 \dots n \quad (5)$$

where  $\underline{u}_i$  and  $\bar{u}_i$  refer to the effectors' lower and upper position limit,  $\dot{\underline{u}}_i$  and  $\dot{\bar{u}}_i$  denote the effectors' lower and upper rate limit,  $\Delta t$  is the control sampling time. Thus, the objective of the control allocation is to find effectors input  $u = [u_1, u_2 \dots u_n]^T$  satisfying the equation (3) within the effectors' physical limits.

Figure 2 illustrates the structure of control allocation framework that we designed. The control allocation distributes the virtual moment commands from upper controller to the redundant effectors, which is composed of four major components, namely effector distribution management scheme, pseudo-inverse, control decoupling and energy-optimized. A brief description of each component is given below. The effector distribution management scheme selects different effectors combination according to current airspeed and tilt angle. The pseudo-inverse uses GI method to calculate the solution of effector input  $u_0$  firstly. Then, the control decoupling module is to handle the cross-coupling effects introduced by thrust vectoring, denoted as  $u_{cor}$ . According to energy model of control effectors that we modelled, energy-optimized model is to give the solution  $u_*$  in order to achieve the minimum-energy effector input of the tiltrotor. Therefore, the effector input signal  $u$  contains three parts as:

$$u = u_0 + u_{cor} + u_* \quad (6)$$

### III. EFFECTOR DISTRIBUTION MANAGEMENT SCHEME

During transition phase, the thrust vectoring and aerodynamic surfaces are all involved in control. we analyze the control effectiveness of effectors with the change of tilt angle and airspeed, then an EDMS based on RCAI is developed to determine the proper switch point between the thrust vectoring and aerodynamic surfaces.

#### A. CONTROL EFFECTIVENESS OF EFFECTORS

The total three-axis moment produced by effectors contain two parts: thrust vectoring and aerodynamic surfaces. As shown in Figure 3,  $O_b - X_b Y_b Z_b$  and  $O_n - X_n Y_n Z_n$  are the same body frame and navigation frame described before.  $O_{mr} - X_{mr} Y_{mr} Z_{mr}$ ,  $O_{ml} - X_{ml} Y_{ml} Z_{ml}$ ,  $O_{mb} - X_{mb} Y_{mb} Z_{mb}$  are rotor frames which are fixed with three rotors, respectively.

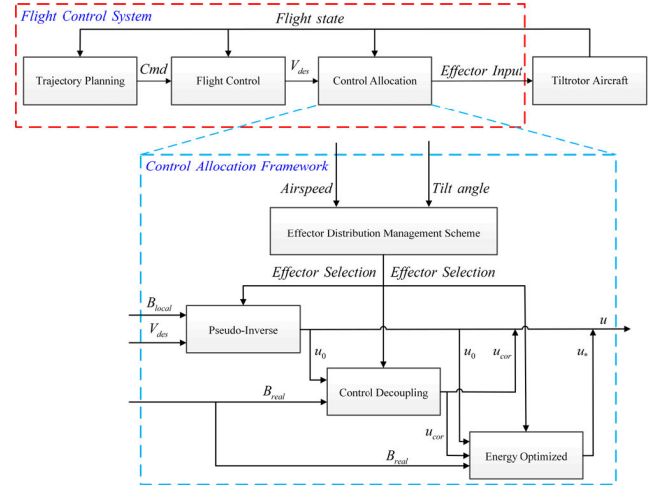


FIGURE 2. Block diagram of the proposed control allocation framework.

Referring to the center of gravity  $O_b$ , the coordinate of right rotor is  $\vec{R}_r = [n, L, 0]^T$ , the left one is  $\vec{R}_l = [n, -L, 0]^T$  and the rear one is  $\vec{R}_b = [-l, 0, h]^T$ .  $O_a - X_a Y_a Z_a$  is velocity reference frame.  $V_a$  is airspeed. The moment generated by thrust vectoring is presented as, shown at the bottom of this page.

where  $[M_{tx}, M_{ty}, M_{tz}]^T$  are roll, pitch and yaw moments of thrust vectoring,  $\vec{T}_r = [T_r \sin A_r, 0, -T_r \cos A_r]^T$ ,  $\vec{T}_l = [T_l \sin A_l, 0, -T_l \cos A_l]^T$ ,  $\vec{T}_b = [0, T_b \sin A_r, -T_b \cos A_r]^T$  are thrust of three rotors expressed in body frame. For convenience of subsequent discussions, the two main rotors' thrust can further be expressed as the function of thrust synchronous component  $T_m$  and thrust differential component  $T_n$ .

$$\begin{bmatrix} T_r \\ T_l \end{bmatrix} = \begin{bmatrix} T_m + T_n \\ T_m - T_n \end{bmatrix} \quad (8)$$

Considering that  $A_r = A_l = A_{rl}$ ,  $h \ll L$ . Rewrite equation (7), as shown at the bottom of the page, as:

$$\begin{bmatrix} M_{tx} \\ M_{ty} \\ M_{tz} \end{bmatrix} \approx \begin{bmatrix} 2L \cdot T_n \cdot \cos A_{rl} \\ -2n \cdot T_m \cdot \cos A_{rl} + l \cdot T_b \cdot \cos A_b \\ 2L \cdot T_n \cdot \sin A_{rl} + l \cdot T_b \cdot \sin A_b \end{bmatrix} \quad (9)$$

Similarly, the two elevons can be expressed as the function of deflection angle of elevator  $A_t$  and deflection angle of aileron  $A_d$ .

$$\begin{bmatrix} A_{ar} \\ A_{al} \end{bmatrix} = \begin{bmatrix} A_t + A_d \\ A_t - A_d \end{bmatrix} \quad (10)$$

$$\begin{aligned} \begin{bmatrix} M_{tx} \\ M_{ty} \\ M_{tz} \end{bmatrix} &= \vec{R}_r \times \vec{T}_r + \vec{R}_l \times \vec{T}_l + \vec{R}_b \times \vec{T}_b \\ &= \begin{bmatrix} y_r \cdot T_r \cdot \cos A_r + y_l \cdot T_l \cdot \cos A_l - z_b \cdot T_b \cdot \sin A_b + y_b \cdot T_b \cdot \cos A_b \\ -z_r \cdot T_r \cdot \sin A_r - z_l \cdot T_l \cdot \sin A_l - x_r \cdot T_r \cdot \cos A_r - x_l \cdot T_l \cdot \cos A_l - x_b \cdot T_b \cdot \cos A_b \\ y_r \cdot T_r \cdot \sin A_r + y_l \cdot T_l \cdot \sin A_l - x_b \cdot T_b \cdot \sin A_b \end{bmatrix} \end{aligned} \quad (7)$$

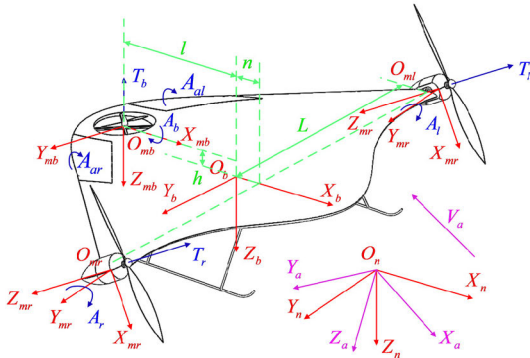


FIGURE 3. The coordinate systems of tiltrotor aircraft.

The moment generated by aerodynamic surfaces are presented as:

$$\begin{bmatrix} M_{mx} \\ M_{my} \\ M_{mz} \end{bmatrix} = \begin{bmatrix} Q \cdot S_w \cdot C_l(p, r, \beta, A_d) \cdot b \\ Q \cdot S_w \cdot C_m(p, q, r, \alpha, A_t) \cdot c_a \\ Q \cdot S_w \cdot C_n(p, r, \beta, A_d) \cdot b \end{bmatrix} \quad (11)$$

where  $[M_{mx}, M_{my}, M_{mz}]^T$  are roll, pitch and yaw moments of aerodynamic surfaces,  $Q = 0.5 \cdot \rho \cdot V_a^2$  is dynamic pressure,  $\rho$  is air density,  $S_w$  is reference wing area,  $b$  is wingspan,  $c_a$  is mean chord,  $(p, q, r)$  are roll, pitch and yaw angular rates,  $C_l(p, r, \beta, A_d)$  is roll moment coefficient related to  $(p, r)$ , sideslip angle  $\beta$  and  $A_d$ ,  $C_m(p, q, r, \alpha, A_t)$  is pitch moment coefficient related to  $(p, q, r)$ , attack angle  $\alpha$  and  $A_t$ ,  $C_n(p, r, \beta, A_d)$  is yaw moment coefficient related to  $(p, r)$ ,  $\beta$  and  $A_d$ . Thus, the total moment can be expressed as, shown at the bottom of this page.

According to equation (2), the local effectiveness matrix  $B_{local}$  is defined as, shown at the bottom of this page.

where  $C_{lA_d} = \partial C_l(p, r, \beta, A_d) / \partial A_d|_{x_0, u_0}$  denotes the roll moment coefficient related to  $A_d$ ,  $C_{mA_t} = \partial C_m(p, q, r, \alpha, A_t) / \partial A_t|_{x_0, u_0}$  denotes the pitch moment coefficient related to  $A_t$ ,  $C_{nA_d} = \partial C_n(p, r, \beta, A_d) / \partial A_d|_{x_0, u_0}$  denotes yaw moment coefficient related to  $A_d$ .

However, different effectors have different operational ranges. For example, the ducted fan operates from 0rpm

to 4000rpm, where the elevator  $A_t$  operates between  $\pm 10^\circ$  ( $\pm \pi / 18 \text{rad}$ ). Obviously, the pitch moment produced per rpm by ducted fan is numerically much smaller than produced per rad by elevator, but it does not mean that the ducted is inefficient due to its larger operational range. Thus, we need to map the effectors input into a unit space before computing the local effectiveness matrix  $B_{local}$ . Assume the  $i$ th effectors' operational range belongs to  $\{u_{i, \min} \leq u_i \leq u_{i, \max}\}$ , the modified effectiveness matrix  $\tilde{B}$  is presented as:

$$\begin{aligned} \tilde{B} &= B_{local} W^{-1}, \tilde{u} = Wu \\ W &= \text{diag} \left[ \frac{1}{u_{i, \max} - u_{i, \min}} \right] \end{aligned} \quad (14)$$

During transition phase, the tiltrotor adopts an inclined-take-off way which increases both the flight height and airspeed. The two main rotors' tilt angle and airspeed (see in Figure 4(a)) are optimized to minimize the take-off time during the trajectory design step. According to equation (13), as shown at the bottom of the page, the control effectiveness of three-axis moments is showed in Figure 4.

As presented in Figure 4(a), the angle of main rotor is deflected from  $0^\circ$  (means VTOL phase) to  $90^\circ$  (means level flight phase), while airspeed grows from 0m/s to 33m/s. Figure 4(b)-4(d) show the control effectiveness of effectors in three channels. For convenience of comparison and description, the effectiveness of effectors is computed with respect to unit effector input (means 1/10 of effectors' operational range).

From Figure 4(b), we can see that the aileron  $A_d$  provides valid roll moment with increase of airspeed and does not have effect on other channel, while the effectiveness of thrust differential component  $T_n$  decreases in roll channel and increases in yaw channel with tilt angle (see in Figure 4(d)). It should be noted that the cross-coupling effects between roll and yaw channel produced by  $T_n$  increases difficulty of control allocation, which we will solve this problem later. The effectiveness of deflection angle of ducted fan  $A_b$  is depressive due to the reduced trimming force of ducted fan. Figure 4(c) shows that the elevator  $A_t$  provides valid pitch

$$\begin{bmatrix} M_x \\ M_y \\ M_z \end{bmatrix} = \begin{bmatrix} M_{tx} + M_{mx} \\ M_{ty} + M_{my} \\ M_{tz} + M_{mz} \end{bmatrix} = \begin{bmatrix} 2L \cdot T_n \cdot \cos A_{rl} + Q \cdot S_w \cdot C_l(p, r, \beta, A_d) \cdot b \\ -2n \cdot T_m \cdot \cos A_{rl} + l \cdot T_b \cdot \cos A_b + Q \cdot S_w \cdot C_m(p, q, r, \alpha, A_t) \cdot c_a \\ 2L \cdot T_n \cdot \sin A_{rl} + l \cdot T_b \cdot \sin A_b + Q \cdot S_w \cdot C_n(p, r, \beta, A_d) \cdot b \end{bmatrix} \quad (12)$$

$$\begin{aligned} B_{local} &= \frac{\partial M}{\partial u} \Big|_{x_0, u_0} = \begin{bmatrix} \frac{\partial M_x}{\partial T_m} & \frac{\partial M_x}{\partial T_n} & \frac{\partial M_x}{\partial T_b} & \frac{\partial M_x}{\partial A_b} & \frac{\partial M_x}{\partial A_t} & \frac{\partial M_x}{\partial A_d} \\ \frac{\partial M_y}{\partial T_m} & \frac{\partial M_y}{\partial T_n} & \frac{\partial M_y}{\partial T_b} & \frac{\partial M_y}{\partial A_b} & \frac{\partial M_y}{\partial A_t} & \frac{\partial M_y}{\partial A_d} \\ \frac{\partial M_z}{\partial T_m} & \frac{\partial M_z}{\partial T_n} & \frac{\partial M_z}{\partial T_b} & \frac{\partial M_z}{\partial A_b} & \frac{\partial M_z}{\partial A_t} & \frac{\partial M_z}{\partial A_d} \end{bmatrix} \Big|_{x_0, u_0} \\ &= \begin{bmatrix} 0 & 2L \cdot \cos A_{rl} & 0 & 0 & 0 & Q \cdot S_w \cdot C_{lA_d} \cdot b \\ 2n \cdot \cos A_{rl} & 0 & -l \cdot \cos A_b & -l \cdot T_b \cdot \sin A_b & Q \cdot S_w \cdot C_{mA_t} \cdot c_a & 0 \\ 0 & 2L \cdot \sin A_{rl} & l \cdot \sin A_b & l \cdot T_b \cdot \cos A_b & 0 & Q \cdot S_w \cdot C_{nA_d} \cdot b \end{bmatrix} \Big|_{x_0, u_0} \end{aligned} \quad (13)$$

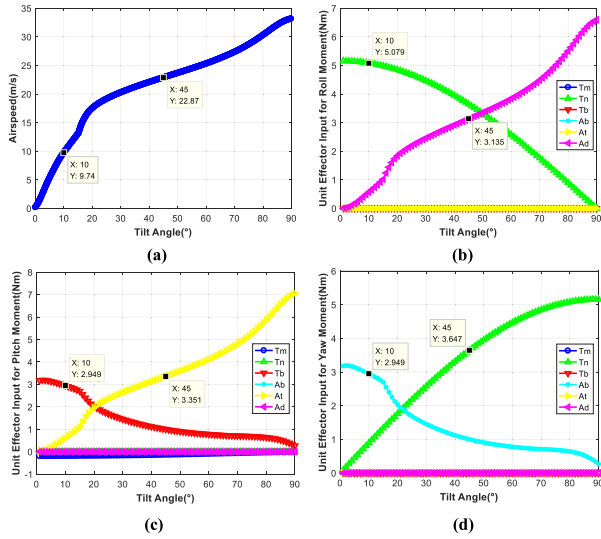


**FIGURE 4. Control effectiveness of effectors in three-axis moments. (a) Airspeed and tilt-angle. (b) Effectiveness of effectors in roll channel. (c) Effectiveness of effectors in pitch channel. (d) Effectiveness of effectors in yaw channel.**

moment with increase of airspeed and has no cross-coupling effect on other channel. The pitch moment produced by ducted fan  $T_b$  also decreases due to the reduced trimming force of ducted fan. The thrust synchronous component  $T_m$  provides small pitch moment due to short distance off the center of gravity.

Conclusively, the effectiveness of effectors is nonlinear and it is important to determine the switch point between thrust vectoring and aerodynamic surfaces.

**B. EFFECTOR DISTRIBUTION MANAGEMENT SCHEME**

The vehicle is more easily subjected to external interference such as wind disturbance due to the larger wing area. As seen in Figure 4(c), the  $A_t$  cannot be included in pitch control channel too early due to its trivial effectiveness, whereas the  $T_b$  cannot provide enough torque to maintain maneuvering capability and resist external interference if  $A_t$  is utilized into the pitch control channel too late. Thus, the improper switch point between the thrust vectoring and aerodynamic surfaces cannot guarantee the control ability of tiltrotor, leading to threat of flight safety. Inspired by the controllability of multirotor systems [38], [39], a RCAI  $\rho(M_{des}, \xi)$  is introduced here to denote the remaining control ability of tiltrotor, which is used to determine the switch point and ensure flight safety.

$$\rho(M_{des}, \xi) \triangleq \begin{cases} \min \left\{ \frac{\|M_{des} - \xi\|}{\xi} : M_{des} \in \Omega, \xi = \max\{\Omega\} \right\} \\ - \min \left\{ \frac{\|M_{des} - \xi\|}{\xi} : M_{des} \in \Omega^C, \xi = \max\{\Omega\} \right\} \end{cases} \quad (15)$$

where  $M_{des}$  denotes moment demand of maneuvering capability,  $\Omega$  denotes constraint set of moment,  $\xi$  denotes the

maximum limit of  $\Omega$ ,  $\Omega^C$  denotes complementary set of  $\Omega$ . When  $\rho(M_{des}, \xi) < 0$  means that  $M_{des}$  exceeds the maximum limit  $\xi$ .

Take the pitch control channel for example, about  $10^\circ$  attack angle change within  $0.7s$  during the transition phase is needed according to trajectory requirement. Therefore, the pitch moment demand  $M_{y,des}$  of maneuvering capability is calculated as:

$$M_{y,des} = J_y \cdot \frac{2\alpha}{t^2} \approx 10Nm \quad (16)$$

where  $J_y$  denotes inertia of y-axis,  $\alpha$  denotes attack angle,  $t$  is variation time. Considering the error of modeling and actual flight conditions, the practical pitch moment is approximately estimated as  $15Nm$ . According to practical engineering experience,  $\rho(M_{des}, \xi) \geq 50\%$  is suitable to resist interference and ensure control margin. As shown in Figure 4(a) and Figure 4(c), the maximum pitch moment produced by  $T_b$  is about  $29.5Nm$  on conditional that tilt angle is  $10^\circ$  and airspeed is  $10m/s$ . The RCAI of  $T_b$  individually at this operating point is about:

$$\rho_{T_b}(M_{des}, \xi) = \|15 - 29.5\|/29.5 \approx 50\% \quad (17)$$

As airspeed and tilt angle grow, it is not difficult to conclude that  $\rho_{T_b}(M_{des}, \xi)$  will below  $50\%$ , thus, the  $A_t$  should be utilized into the pitch control channel from this operating point which can guarantee the requirement of  $\rho(M_{des}, \xi) \geq 50\%$ . The maximum pitch moment produced by  $A_t$  individually is about  $33Nm$  when the tilt angle is  $45^\circ$  and airspeed is  $23m/s$ . The  $\rho_{A_t}(M_{des}, \xi)$  individually at this point is  $54\%$  over  $50\%$ . Thus, this operating point is taken as the time that the ducted fan exits pitch control channel.

The same method can be used to analysis the roll and yaw control channel, as the length limit, the detailed analysis will not discuss here. The whole effector distribution management scheme for all flight phases is summarized in Table 3.

**IV. ENERGY OPTIMIZED CONTROL ALLOCATION**

During transition II phase, thrust vectoring and aerodynamic surfaces are mixed for control. The energy consumption of effectors varies with the change of airspeed and tilt angel. This section further introduces the detailed energy model of control effectors and three procedures of energy optimized control allocation.

**A. ENERGY MODEL OF CONTROL EFFECTORS**

**1) THRUST VECTORING ENERGY MODE**

This novel tiltrotor adopts a typical propulsion system which consists of a battery pack, an electronic speed control (ESC), a brushless direct-current motor, and a propeller. The energy transmission diagram of this vehicle’s propulsion system is shown in Figure 5.

According to [40], a widely used index called thrust efficiency  $\eta_m$ (unit:  $g/W$ ) is introduced here to describe the power

**TABLE 3. Effector distribution management scheme.**

Flight phase	Operating range	Control effectors
Vertical takeoff and landing	Tilt angle < 5°, Airspeed < 5m/s	Pitch channel: $T_b$
		Roll channel: $T_n$
		Yaw channel: $A_b$
Transition I	Tilt angle < 10°, Airspeed < 10m/s	Pitch channel: $T_b$
		Roll channel: $T_n$
		Yaw channel: $A_b$
Transition II	10° < Tilt angle < 45°, 10m/s < Airspeed < 23m/s	Pitch channel: $T_b$ and $A_i$
		Roll channel: $T_n$ and $A_d$
		Yaw channel: $A_b$ and $T_n$
Transition III	45° < Tilt angle < 90°, 23m/s < Airspeed < 33m/s	Pitch channel: $A_i$
		Roll channel: $A_d$
		Yaw channel: $T_n$
Level flight	Tilt angle = 90°, Airspeed > 33m/s	Pitch channel: $A_i$
		Roll channel: $A_d$
		Yaw channel: $T_n$

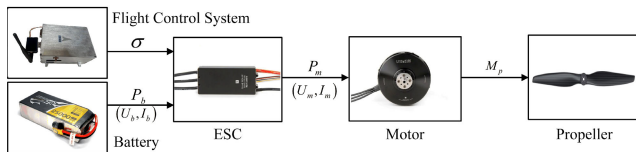


**FIGURE 5. Energy transmission diagram of propulsion system.**

consumption of the thrust vectoring.

$$\eta_m = \frac{T_p}{P_b} = \frac{T_p}{U_b \cdot I_b} = f(\Theta_P, \Theta_M, \Theta_B, \Theta_E) \quad (18)$$

where  $T_p$  denotes the propeller output thrust,  $P_b$  denotes output power of battery,  $U_b$  and  $I_b$  are working voltage and current of battery.  $\Theta_P$  are propeller parameters related to blade diameter, pitch angle and blade number.  $\Theta_M$  are motor parameters related to KV value, continuous working current and inherent resistance.  $\Theta_B$  are battery parameters related to capacity and nominal voltage.  $\Theta_E$  are environment parameters related to air density and temperature.

For this novel tiltrotor, ground effect is an important factors which may affect the thrust efficiency  $\eta_m$  of three propellers. According to [41], [42] and computational fluid dynamics analysis of the tiltrotor, the thrust of propeller  $T_g$  considering the effect of ground can be calculated as:

$$\begin{cases} \frac{T_g}{T} = 1 + 0.01x^{(1+0.5x)} \\ x = 4 - \frac{10}{3} \left( \frac{H}{D} \right) \end{cases} \quad (19)$$

where  $T$  is thrust of propeller faraway from ground effect,  $H$  is the height of propeller above ground,  $D$  is the diameter of propeller. The influence of ground effect  $T_g/T$  on propeller thrust with respect to  $H/D$  can be further illustrated in Figure 6.

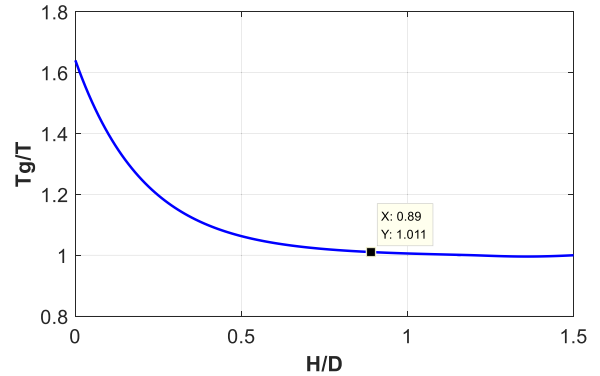


**FIGURE 6. The influence of ground effect on propeller.**



**FIGURE 7. The configuration of rear ducted fan.**

The propeller diameter of this tiltrotor is 910mm, while the height of propeller above ground is about 800mm, according to equation (19),  $T_g/T \approx 1.011$ . Considering that the height  $H$  will increase as vehicle takes off, the  $T_g/T$  will be close to 1. Thus, the influence of ground effect on propeller thrust can be ignored. Besides this, the rear rotor adopts ducted fan configuration (see Figure 7), which will increase efficiency. Thus, we will build a look-up table of thrust efficiency using real flight data for after calculation.

## 2) AERODYNAMIC SURFACES ENERGY MODE

The aerodynamic surfaces driven by tilting servos require different power consumption with different deflection angle. The energy transmission diagram of this vehicle's aerodynamic surfaces system is shown in Figure 8.

Similarly, an index called “deflection angle efficiency”  $\eta_w \eta_m$  (unit: rad/W) is introduced to describe the power consumption of the aerodynamic surfaces.

$$\eta_w = \frac{\delta_w}{P_s} = \frac{\delta_w}{U_s \cdot I_s} = f(X, \Theta_W, \Theta_S) \quad (20)$$

where  $\delta_w$  denotes the deflection angle of aerodynamic surfaces,  $P_s$  denotes output power of servo battery,  $U_s$  and  $I_s$  are working voltage and current of servo battery.  $X$  are flight states related to airspeed, air density and height.  $\Theta_W$  are aerodynamic surfaces' parameters related to wing area, weight and airfoil.  $\Theta_S$  are servo parameters related to nominal voltage, current and speed.

Differing from the thrust vectoring, the working voltage and current of servo battery cannot be measured directly due

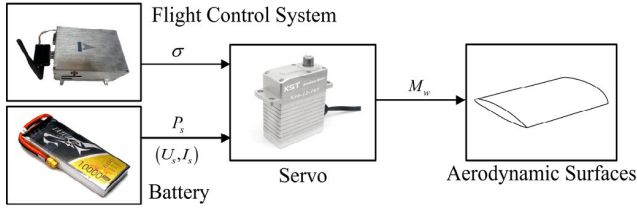


FIGURE 8. Energy transmission diagram of aerodynamic surfaces.

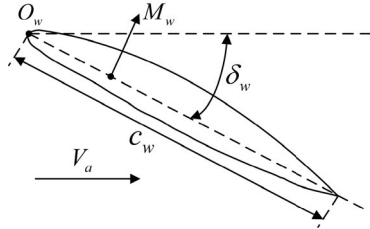


FIGURE 9. Aerodynamic load of aerodynamic surfaces.

to limited space of aircraft. Thus, a practical method is developed to estimate the power consumption of aerodynamic surfaces. The aerodynamic surfaces subjected to aerodynamic load, gravity load and friction moment will generate a hinge moment of servo. According to [43], the aerodynamic load (see Figure 9) is the main source of hinge moment  $M_w$ , which can be modeled as:

$$M_w = C_w Q S_w c_w \delta_w \quad (21)$$

where  $C_w$  is the hinge moment coefficient,  $Q$  is dynamic pressure,  $S_w$  is the reference area of aerodynamic surface,  $c_w$  is the mean chord of rudder,  $\delta_w$  is the deflection angle of aerodynamic surface. After we obtain the  $M_w$ , the power consumption of servo can be calculated using the curve of torque-power which will be described in latter part.

## B. ENERGY OPTIMIZED CONTROL ALLOCATION

### 1) PSEUDO-INVERSE

GI method is found to be effective and computationally efficient to implement for real-time flight control system. Moore-Penrose inverse is a special generalized inverse which provides a solution with minimum norm. Considering that the practical flight control system usually adopts a discrete periodic calculating method. Thus, the optimization objective is chosen as the error of effector input between current cycle  $k$  and last cycle  $k - 1$ .

$$J = \min \|u(k) - u(k - 1)\|_2 \quad (22)$$

*s.t.*  $B_{local}u(k) = v_{des}$

Define the error of effector input  $e$  between current cycle  $k$  and last cycle  $k - 1$  as:

$$e = u(k) - u(k - 1) \quad (23)$$

Rewrite equation (23) as:

$$u(k) = u(k - 1) + e \quad (24)$$

Combine with equation (22) and (24), the optimization objective is written as:

$$J = \min \|e\|_2 \quad (25)$$

*s.t.*  $B_{local}(u(k - 1) + e) = v_{des}$

$\Downarrow$

$$B_{local}e = v_{des} - B_{local}u(k - 1)$$

Here, Moore-Penrose inverse is utilized to calculate the minimum solution.

$$u(k) - u(k - 1) = (B_{local})^+ (v_{des} - B_{local}u(k - 1))$$

$$u(k) = \underbrace{(I - (B_{local})^+ B_{local})}_{F} u(k - 1) + \underbrace{(B_{local})^+}_{P} v_{des} \quad (26)$$

Thus, the analytical solution of equation (22) is:

$$u(k) = Fu(k - 1) + Pv_{des} \quad (27)$$

$$F = I - PB_{local}, P = (B_{local})^+ = B_{local}^T (B_{local}B_{local}^T)^{-1}$$

### 2) CONTROL DECOUPLING

Differing from conventional aircraft configuration, the thrust vectoring would introduce cross-coupling effects in control allocation. Firstly, the thrust  $T_b$  and deflection angle  $A_b$  of ducted fan would produce the coupling effect between pitch and yaw control channel during VTOL phase. Secondly, the control efficient of effector  $T_n$  would transfer from roll channel to yaw channel with the tilt angle during transition phase. Actually, the  $B_{local}$  used in Pseudo-Inverse ignores the cross-coupling elements of  $B_{real}$ , which obviously introduces error. The control decoupling algorithm is meant to correct this coupling error. The real control matrix  $B_{real}$  can be expressed as:

$$B_{real} = B_{local} + B_{err} \quad (28)$$

where  $B_{err}$  contains the cross-coupling elements. The solution from Pseudo-Inverse  $u(k)$  is denoted as  $u_0$ . Thus, the actual achieved moment  $v_{real}$  is:

$$v_{real} = B_{real}u_0 = (B_{local} + B_{err})u_0 = \underbrace{B_{local}u_0}_{v_{des}} + \underbrace{B_{err}u_0}_{v_{err}} \quad (29)$$

where  $v_{err} = B_{err}u_0$  denotes the error introduced by cross-coupling effects. We desire to find another  $u_{cor}$  to correct this error.

$$v_{real} = B_{real}(u_0 + u_{cor}) = v_{des}$$

$\Downarrow$

$$B_{local}(u_0 + u_{cor}) + B_{err}(u_0 + u_{cor}) = v_{des}$$

$\Downarrow$

$$B_{local}u_{cor} + B_{err}(u_0 + u_{cor}) = 0$$

$\Downarrow$

$$B_{err}u_0 + B_{real}u_{cor} = 0 \quad (30)$$



Given  $B_{real}$ ,  $B_{err}$  and  $u_0$ , the correct norm  $u_{cor}$  is easy to calculate as:

$$u_{cor} = -(B_{real})^+ B_{err} u_0 \quad (31)$$

where  $(B_{real})^+$  denotes Moore-Penrose inverse of  $B_{real}$ . Furthermore, the effector input can be written as:

$$\begin{aligned} u_1 &= u_0 + u_{cor} = u_0 - (B_{real})^+ B_{err} u_0 \\ &= (I - (B_{real})^+ B_{err}) u_0 \end{aligned} \quad (32)$$

### 3) ENERGY OPTIMIZED METHOD BASED ON NULL SPACE TRANSITION

Here, the energy optimized method based on null space transition is designed to find the minimum-energy solution for this vehicle.

Define the number of effectors is  $n$ ,  $r$  is rank of effectiveness matrix  $B_{real} \in R^{3 \times n}$ , thus,  $m = n - r$  is the redundant degree of effectors. The effector input staying in the null space of effectiveness matrix  $B_{real}$  denotes as  $u_*$ . The total input  $u$  can be expressed as:

$$u = u_1 + u_* \quad s.t. \quad B_{real} u = B_{real} (u_1 + u_*) = B_{real} u_1 \quad (33)$$

Define  $[S] = [s_1^T \ s_2^T \ \dots \ s_m^T]^T \in R^{n \times m}$  is the orthogonal basis of null space of effectiveness matrix  $B_{real}$ ,  $\lambda = [\lambda_1 \ \lambda_2 \ \dots \ \lambda_m] \in R^{m \times 1}$  is the scale coefficient of orthogonal basis  $[S]$ . An arbitrary vector in the null space can be written as  $u_* = [S] \lambda$ . The goal is to find a group of optimal coefficient  $\lambda$  which makes the energy index of effector minimum. The relationship between energy consumption  $P = [P_1 \ P_2 \ \dots \ P_6]$  and effectors input is:

$$P = \begin{bmatrix} 1/\eta_{T_n} & 0 & 0 & 0 & 0 & 0 \\ 0 & 1/\eta_{T_m} & 0 & 0 & 0 & 0 \\ 0 & 0 & 1/\eta_{T_b} & 0 & 0 & 0 \\ 0 & 0 & 0 & 1/\eta_{A_b} & 0 & 0 \\ 0 & 0 & 0 & 0 & 1/\eta_{A_t} & 0 \\ 0 & 0 & 0 & 0 & 0 & 1/\eta_{A_d} \end{bmatrix} \begin{bmatrix} T_n \\ T_m \\ T_b \\ A_b \\ A_t \\ A_d \end{bmatrix} \quad (34)$$

where  $\eta_i$ ,  $i = T_n, T_m, T_b, A_b, A_t, A_d$  are energy coefficient described above. And furthermore, the energy index of effector is defined as:

$$J = \frac{1}{2} \|P\|_2^2 = \frac{1}{2} \sum_{i=1}^n P_i^2 = \frac{1}{2} P^T P \quad (35)$$

Combined with equation (33), we can obtain:

$$\begin{aligned} J &= \frac{1}{2} (\eta (u_1 + u_*))^T (\eta (u_1 + u_*)) \\ &= \frac{1}{2} (\eta (u_1 + [S] \lambda))^T (\eta (u_1 + [S] \lambda)) \end{aligned} \quad (36)$$

The optimal coefficient  $\lambda$  should be determined satisfying the two follow conditions:

$$\begin{cases} \frac{\partial J}{\partial \lambda} = 0 \\ \frac{\partial^2 J}{\partial \lambda^2} > 0 \end{cases} \quad (37)$$

According to (36), the derivative of  $J$  with respect to  $\lambda$  is written as:

$$\begin{aligned} \frac{\partial J}{\partial \lambda} &= (\eta (u_1 + [S] \lambda))^T \eta [S] = 0 \\ [S]^T \eta^2 [S] \lambda &= -[S]^T \eta^2 u_1 \end{aligned} \quad (38)$$

Considering that the basis vector of  $[S]$  is not zero vector, thus, the matrix  $[S]^T \eta^2 [S]$  can be written as:

$$[S]^T \eta^2 [S] = \sum_{i=1}^n \eta_i^2 s_i s_i^T = A \quad (39)$$

It is obvious that the  $\eta_i^2$  of any effector has  $\eta_i^2 > 0$ , thus, it means that the rank of matrix  $A$  is  $m$  and  $A$  is invertible. However,  $\partial J / \partial \lambda = 0$  is only the extremum condition. In order to guarantee the minimum energy,  $\partial^2 J / \partial \lambda^2$  must be a positive definite matrix, which means  $\partial^2 J / \partial \lambda^2 > 0$ . The two-order derivative of  $J$  can be written as:

$$\frac{\partial^2 J}{\partial \lambda^2} = [S]^T \eta^2 [S] = \sum_{i=1}^n \eta_i^2 s_i s_i^T = A \quad (40)$$

From the above analysis, we can see  $\partial^2 J / \partial \lambda^2 = A > 0$ . It means that the optimal coefficient  $\lambda$  which guarantees the minimum energy is calculated as:

$$\lambda = -[S]^T \eta^2 [S]^{-1} [S]^T \eta^2 u_1 \quad (41)$$

Furthermore, we can obtain the total effector input as:

$$\begin{aligned} u &= u_0 + u_{cor} + u_* = u_1 - [S] [S]^T \eta^2 [S]^{-1} [S]^T \eta^2 u_1 \\ &= \left( I - [S] [S]^T \eta^2 [S]^{-1} [S]^T \eta^2 \right) u_1 \\ &= \left( I - [S] [S]^T \eta^2 [S]^{-1} [S]^T \eta^2 \right) \\ &\quad \times \left( I - (B_{real})^+ B_{err} \right) u_0 \end{aligned} \quad (42)$$

## V. EXPERIMENTAL RESULTS

For verifying the effectiveness of the proposed method, some model parameters need to be measured firstly.

### A. ENERGY MODEL PARAMETERS MEASUREMENTS

#### 1) THRUST VECTORING MODEL PARAMETER

The propeller output thrust  $T$  is controlled by the throttle signal  $\sigma \in [0, 1]$  of flight control system. The relation between  $T$  and  $\sigma$  is measured by the test benches. The test benches can precisely measure the input voltage, current and the output rotating speed, thrust of the propeller, which is convenient to fit the relation. The test bench and fitting curve are shown in Figure 10.

The relation between thrust  $T_{rl}$  of two main rotors and throttle signal  $\sigma_{rl}$  is fitted by least square method as:

$$T_{rl} = 104 \sigma_{rl}^2 \quad (43)$$

Similarly, the thrust of rear ducted fan  $T_b$  is:

$$T_b = 8 \sigma_b^2 \quad (44)$$

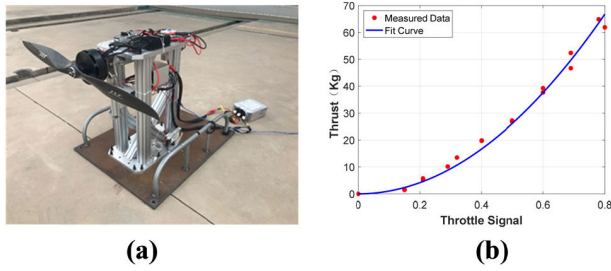


FIGURE 10. The propulsion system of tiltrotor aircraft. (a) Test beaches. (b) Fitting curve.

where  $\sigma_b$  is throttle signal of ducted fan. Considering that the ESC actually accepts PWM signal, a reverse transformation is conducted to calculate the PWM signal  $u_p$  (unit: us):

$$u_p = 1100 + 750 \times \sigma \quad (45)$$

Besides this, proper sensors such as voltage and current sensors are installed in the vehicle to monitor the real-time working voltage and current. Considering that the thrust efficiency is not a constant, which is affected by the working state of propulsion system. Thus, we utilize test data of beaches and a real flight data (see Figure 11) to build a look-up table of thrust efficiency.

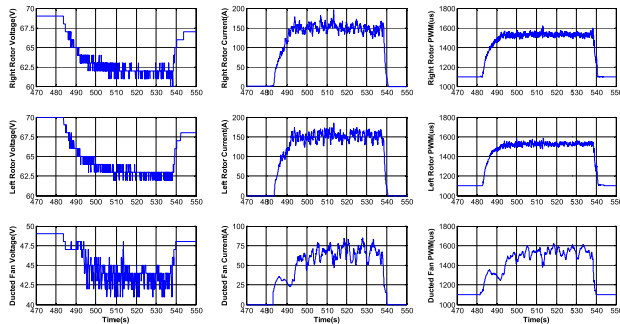


FIGURE 11. The PWM signal, voltage and current of real flight data.

According to equation (18) and equation (43-45), the look-up table of thrust efficiency of three rotors is shown in Table 4.

2) AERODYNAMIC SURFACES MODEL PARAMETER

The Aerodynamic surfaces driven by the tilting servo (see Figure 12(a)) accept PWM signal  $u_{servo} \in [1000, 2000]$  us of flight control system. Before calculating the “deflection angle efficiency”  $\eta_w$  described above, we need to identify the relation between deflection angle  $\delta_w$  and PWM signal  $u_{servo}$ . The deflection angle  $\delta_w$  is measured by CPLD and photoelectric encoder whose measuring accuracy is about  $0.1^\circ$ . The relation between deflection angle  $\delta_w$  and PWM signal  $u_{servo}$  is fitted by least square method as:

$$\delta_w = (u_{servo} - 1000) \times 0.0923707812 \quad (46)$$

The parameters related to hinge moment of servo  $M_w$  such as  $C_w$ ,  $S_w$  and  $c_w$  can be obtained by computational fluid dynamics. After calculating the  $M_w$ , the power consumption of servo can be calculated using the curve of torque-power (see Figure 12(b)) which is fitted by test data.

TABLE 4. Thrust efficiency of three rotors.

Rotor	Throttle signal	Thrust efficiency(g/W)
Right rotor	0.1	4.98
	0.2	4.54
	0.3	4.21
	0.4	3.84
	0.5	3.63
	0.6	3.28
	0.7	2.98
	0.8	2.81
	0.9	2.61
	1.0	2.25
Left rotor	0.1	5.03
	0.2	4.62
	0.3	4.28
	0.4	3.87
	0.5	3.69
	0.6	3.38
	0.7	3.08
	0.8	2.79
	0.9	2.58
	1.0	2.29
Rear ducted fan	0.1	1.79
	0.2	1.69
	0.3	1.61
	0.4	1.49
	0.5	1.40
	0.6	1.33
	0.7	1.26
	0.8	1.21
	0.9	1.15
	1.0	1.08

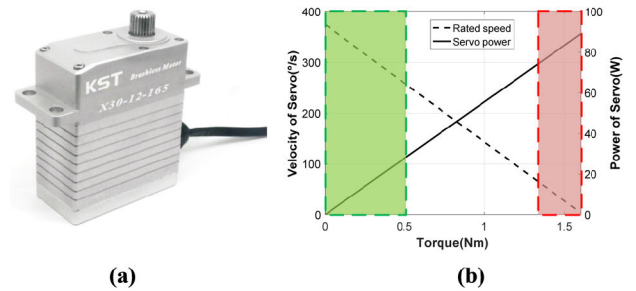


FIGURE 12. The servo of tiltrotor aircraft. (a) Servo. (b) Curve of torque-power.

B. CONTROL ALLOCATION METHOD VERIFICATION

1) EXPERIMENTAL SETUP

In this part, a real-time hardware-in-loop simulation platform is adopted to evaluate the performance of proposed control allocation method for safety considerations. The platform is shown in Figure 13.

The platform consists of five parts: a master computer, a self-developed flight controller, a tiltrotor aircraft, a RC transmitter and a ground station. The master computer acts as the core of the whole simulation platform, which accepts RC and user command, monitors effector state of tiltrotor aircraft and generates simulated navigation data to flight controller by a high-fidelity tiltrotor dynamic model and environment model. The flight controller mainly runs the proposed control allocation algorithm and generates effector command to

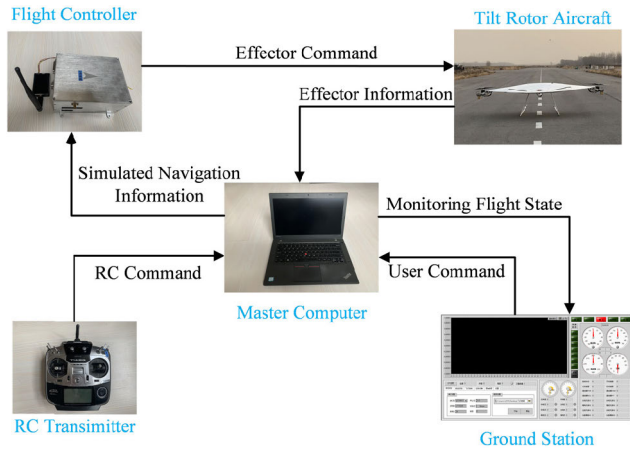


FIGURE 13. The real-time hardware-in-loop simulation platform.

tiltrotor aircraft. In order to simulate and observe the real execution action of effectors, the tiltrotor accepts effectors' command to execute the corresponding action. The ground station can communicate with master computer and display the flight state. The RC transmitter can send some command to perform the emergency task.

We involved as much hardware and software as possible in the simulation platform, which are really used on our tiltrotor. Although the tiltrotor dynamic model cannot match the real vehicle completely, we endeavor to utilize ground-based tests and actual flight results to improve the accuracy of simulation platform, which ensure enough credibility.

2) EXPERIMENTAL TESTS RESULTS

Figure 14 demonstrates the three-dimensional flying trajectory and airspeed during the whole flight. As seen in Figure 14, the whole flight can be divided into four parts: the VTOL, transition I, transition II and transition III. The corresponding effectors of four parts can be found in Table 3. The vehicle hovers at 0m for 5s and then starts to adopt an inclined-take-off way for 35s which increases both the flight height and airspeed. After climbing to 40m height, the vehicle turns to the level flight in 33m/s airspeed.

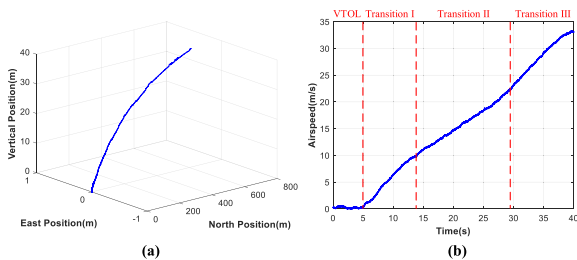


FIGURE 14. Three-dimensional flying trajectory and airspeed. (a) Flying trajectory. (b) Airspeed.

The Figure 15 shows the flight results of attitude. The roll and yaw angles keep to 0°. The pitch angle keeps to the maximum 10° to start transition from 5s. As the airspeed grows, the pitch angle decreases gradually which still remains 2° to provide proper attack angle for level flight.

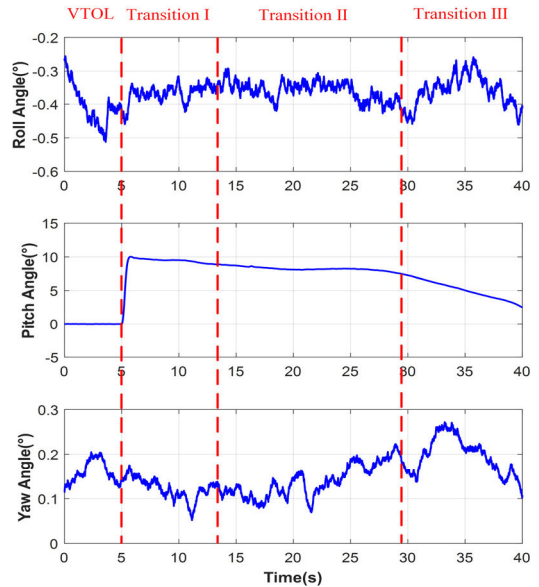


FIGURE 15. The results of attitude.

The effectors' behaviors and the correspond PWM commands are shown in Figure 16-Figure 18. As seen in Figure 16, the angle of two main rotors varies from 0° to 90° during the whole flight. The thrust of three rotors are shown in Figure 17. It is easy to see that the two main rotors which are designed to provide lift (about 31Kg) for hover, decreases gradually to about 3Kg with the change of airspeed and tilt angle, because of only overcoming drag in level flight. The thrust of ducted fan decreases to 0Kg from the beginning of transition III due to its lower control efficiency.

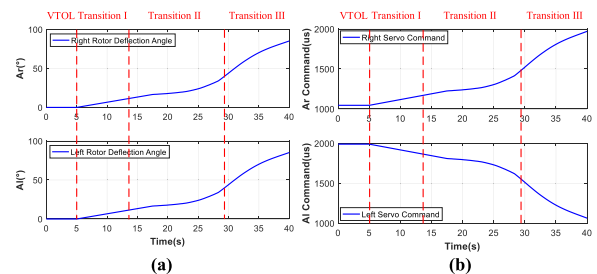


FIGURE 16. The effector input of two main rotors. (a) Deflection angle. (b) PWM command.

As shown in Figure 18, the aerodynamic surfaces mixed with thrust vectoring are utilized to produce pitch and roll moment from the beginning of transition II, which is accordance with the effector distribution management scheme described before. When the vehicle reaches 23m/s, the elevon is used in pitch and roll control independently and the deflection angle of ducted fan exits the yaw control during transition III.

The thrust vectoring and aerodynamic surfaces are mixed in controlling during transition II phase. Thus, the energy consumption of proposed method and traditional PI method during transition II are shown in Figure 19. The energy

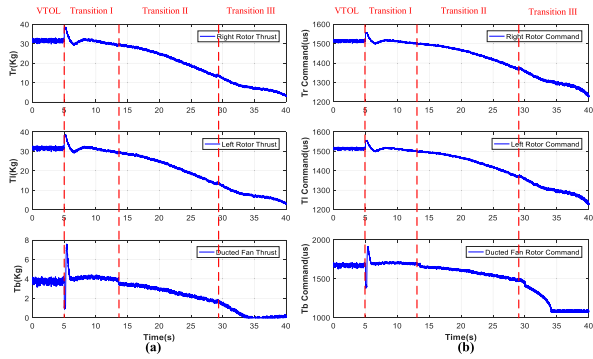


FIGURE 17. The effector input of three rotors. (a) Thrust. (b) PWM command.

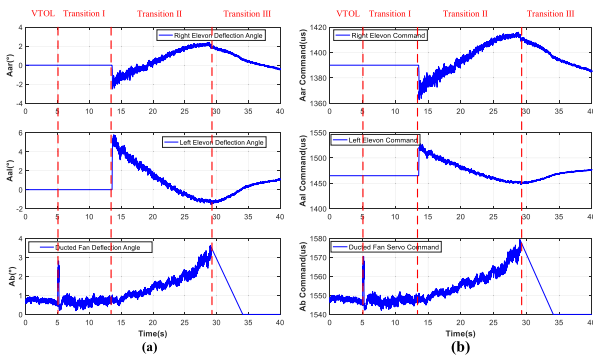


FIGURE 18. The effector input of aerodynamic surfaces. (a) Deflection angle. (b) PWM command.

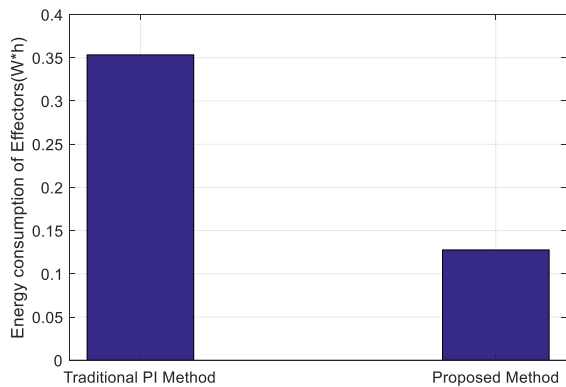


FIGURE 19. The energy consumption of proposed method and traditional PI.

consumption of proposed method reduces by about 63.5% comparing to traditional GI method.

For a more intuitive comparison of two methods, the effectors actions in three-axis control channel during transition II phase are illustrated in Figure 20-22. Without loss of generality, the roll channel was analyzed. From Figure 20, we can see that the aileron  $A_d$  and thrust differential component  $T_n$  are both used in roll channel. The proposed energy-optimized method improves the deflection angle of  $A_d$ , while reduces the input of  $T_n$ , which is in accordance with a fact that the energy consumption of aerodynamic surfaces is lower than thrust vectoring in current flight state. The same analysis method can be used in pitch and yaw channel.

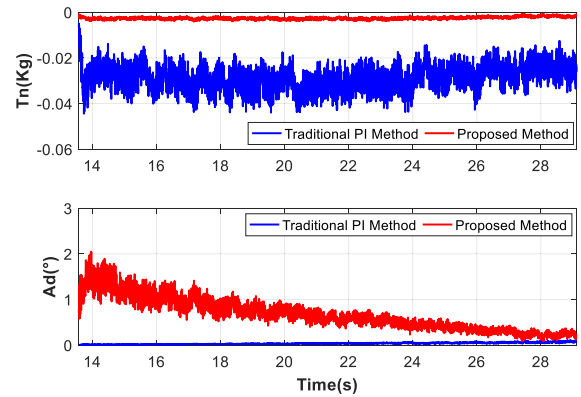


FIGURE 20. Effectors actions in roll control channel.

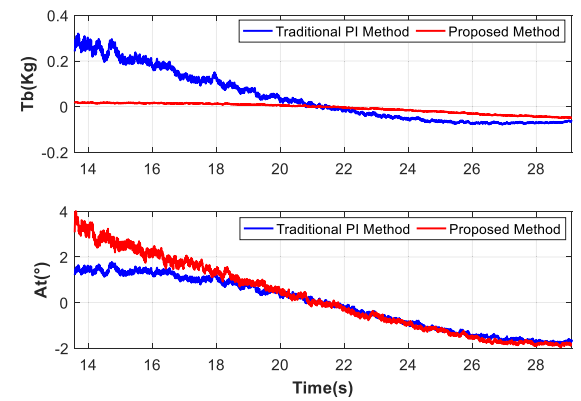


FIGURE 21. Effectors actions in pitch control channel.

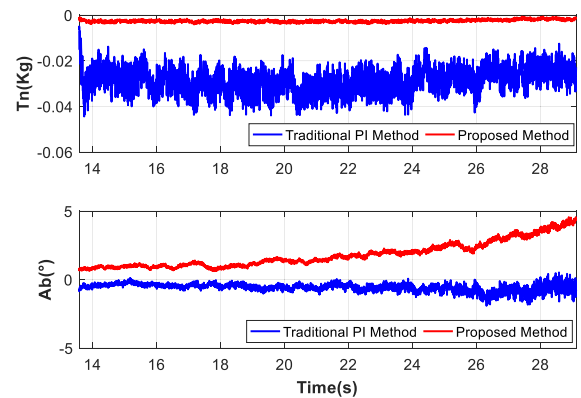


FIGURE 22. Effectors actions in yaw control channel.

## VI. CONCLUSION

This paper proposes a control allocation framework for the novel tiltrotor to solve the problem of three-axis moment distribution. The proposed method makes attempt to take flight safety into consideration during the design process of control allocation which is distinguishing from traditional method. More specifically, the EDMS based on RCAI determines the proper switch point between the thrust vectoring and aerodynamic surfaces which can reduce the effector saturation and ensure flight safety. This control allocation framework is easy to be extended to other configuration of tiltrotor aircraft. Besides this, the energy consumption

models for two classes of effectors are discussed. Then the null space transition is used to give the minimum-energy solution under the premise of allocation precision. Another feature in the proposed method is the control decoupling algorithm which aims to address the cross-coupling problem. Finally, the real-time hardware-in-loop simulation platform is adopted to demonstrate the effectiveness of the proposed control allocation framework. Experimental results show that the energy consumption of proposed method can reduce by about 63.5% comparing to traditional method. Although the actuator dynamics of this tiltrotor is fast enough to be ignored, different kinds of effectors such as thrust vectoring and aerodynamic surfaces have different bandwidths. Thus, the influence of actuator dynamics on control allocation will be investigated in future.

## REFERENCES

- M. Sato and K. Muraoka, "Flight controller design and demonstration of quad-tilt-wing unmanned aerial vehicle," *J. Guid., Control, Dyn.*, vol. 38, no. 6, pp. 1071–1082, Jun. 2015.
- B. Yuksek, A. Vuruskan, U. Ozdemir, M. A. Yukselen, and G. Inalhan, "Transition flight modeling of a fixed-wing VTOL UAV," *J. Intell. Robot. Syst.*, vol. 84, nos. 1–4, pp. 83–105, Jan. 2016.
- B. Li, W. F. Zhou, J. X. Sun, C. Y. Wen, and C. K. Chen, "Development of model predictive controller for a Tail-Sitter VTOL UAV in hover flight," *Sensors*, vol. 18, no. 9, pp. 2859–2879, Aug. 2018.
- K.-J. Nam, J. Joung, and D. Har, "Tri-copter UAV with individually tilted main wings for flight maneuvers," *IEEE Access*, vol. 8, pp. 46753–46772, 2020.
- Z. Liu, Y. He, L. Yang, and J. Han, "Control techniques of tilt rotor unmanned aerial vehicle systems: A review," *Chin. J. Aeronaut.*, vol. 30, no. 1, pp. 135–148, Feb. 2017.
- Z. Wu, C. Li, and Y. Cao, "Numerical simulation of Rotor-Wing transient interaction for a Tiltrotor in the transition mode," *Mathematics*, vol. 7, no. 2, p. 116, Jan. 2019.
- W. C. Durham, "Constrained control allocation—Three-moment problem," *J. Guid., Control, Dyn.*, vol. 17, no. 2, pp. 330–336, Mar. 1994.
- O. Härkegård and S. T. Glad, "Resolving actuator redundancy—Optimal control vs. control allocation," *Automatica*, vol. 41, no. 1, pp. 137–144, Jan. 2005.
- T. A. Johansen and T. I. Fossen, "Control allocation—A survey," *Automatica*, vol. 49, no. 5, pp. 1087–1103, May 2013.
- P. Zheng, X. Tan, B. B. Kocer, E. Yang, and M. Kovac, "TiltDrone: A fully-actuated tilting quadrotor platform," *IEEE Robot. Autom. Lett.*, vol. 5, no. 4, pp. 6845–6852, Oct. 2020.
- M. Furci, D. Bicego, and A. Franchi, "Design and input allocation for robots with saturated inputs via genetic algorithms," in *Proc. 12th IFAC Symp. Robot Control (SYROCO)*, Budapest, Hungary, 2018, pp. 459–464.
- G. Michieletto, M. Ryll, and A. Franchi, "Fundamental actuation properties of multirotors: Force-moment decoupling and fail-safe robustness," *IEEE Trans. Robot.*, vol. 34, no. 3, pp. 702–715, Jun. 2018.
- M. Kamel, S. Verling, O. Elkhatib, C. Sprecher, P. Wulkop, Z. Taylor, R. Siegwart, and I. Gilitschenski, "The voliro omniorientational hexacopter: An agile and maneuverable tiltable-rotor aerial vehicle," *IEEE Robot. Autom. Mag.*, vol. 25, no. 4, pp. 34–44, Dec. 2018.
- Y. Yan, J. Yang, C. Liu, M. Coombes, S. Li, and W.-H. Chen, "On the actuator dynamics of dynamic control allocation for a small fixed-wing UAV with direct lift control," *IEEE Trans. Control Syst. Technol.*, vol. 28, no. 3, pp. 984–991, May 2020.
- H. Alwi and C. Edwards, "Fault tolerant control using sliding modes with on-line control allocation," *Automatica*, vol. 44, no. 7, pp. 1859–1866, Jul. 2008.
- J. Jin, "Modified pseudoinverse redistribution methods for redundant controls allocation," *J. Guid., Control, Dyn.*, vol. 28, no. 5, pp. 1076–1079, Sep. 2005.
- D. Enns, D. Bugajski, R. Hendrick, and G. Stein, "Dynamic inversion: An evolving methodology for flight control design," *Int. J. Control*, vol. 59, no. 1, pp. 71–91, Jan. 1994.
- C. Chen, J. Y. Zhang, D. B. Zhang, and L. C. Shen, "Control and flight test of a tilt-rotor unmanned aerial vehicle," *Int. J. Adv. Robot. Syst.*, vol. 14, no. 1, pp. 1–12, Jan. 2017.
- M. Yayla, A. T. Kutay, M. Senipek, and O. Gungor, "An adaptive flight controller design for a tilt-prop fixed wing UAV for all flight modes," in *Proc. AIAA Scitech Forum*, Orlando, FL, USA, Jan. 2020, pp. 1–20.
- Z. Wang, J. Li, and D. Duan, "Manipulation strategy of tilt quad rotor based on active disturbance rejection control," *Proc. Inst. Mech. Eng., G, J. Aerosp. Eng.*, vol. 234, no. 3, pp. 573–584, Sep. 2019.
- L. Meier, P. Tanskanen, L. Heng, G. H. Lee, F. Fraundorfer, and M. Pollefeys, "PIXHAWK: A micro aerial vehicle design for autonomous flight using onboard computer vision," *Auto. Robots*, vol. 33, nos. 1–2, pp. 21–39, Feb. 2012.
- Z. Chen and H. Jia, "Design of flight control system for a novel tilt-rotor UAV," *Complexity*, vol. 2020, Mar. 2020, Art. no. 4757381.
- D. Rohr, T. Stastny, S. Verling, and R. Siegwart, "Attitude and cruise control of a VTOL tiltwing UAV," *IEEE Robot. Autom. Lett.*, vol. 4, no. 3, pp. 2683–2690, Jul. 2019.
- G. D. Francesco and M. Mattei, "Modeling and incremental nonlinear dynamic inversion control of a novel unmanned tiltrotor," *J. Aircr.*, vol. 53, no. 1, pp. 73–86, Jan. 2016.
- T. Lombaerts, J. Kaneshige, S. Schuet, G. Hardy, B. L. Aponso, and K. H. Shish, "Nonlinear dynamic inversion based attitude control for a hovering quad tiltrotor eVTOL vehicle," in *Proc. AIAA Scitech Forum*, San Diego, CA, USA, Jan. 2019, pp. 1–26.
- Z. Wang, Z. Gong, Y. Chen, M. Sun, and J. Xu, "Practical control implementation of tri-tiltRotor flying wing unmanned aerial vehicles based upon active disturbance rejection control," *Proc. Inst. Mech. Eng., G, J. Aerosp. Eng.*, vol. 234, no. 4, pp. 943–960, Mar. 2020.
- J. Zhang, P. Bhardwaj, S. A. Raab, S. Saboo, and F. Holzappel, "Control allocation framework for a tilt-rotor vertical take-off and landing transition aircraft configuration," in *Proc. Appl. Aerodynamics Conf.*, Atlanta, GA, USA, Jun. 2018, pp. 1–29.
- P. A. Servidia and R. S. Pena, "Spacecraft thruster control allocation problems," *IEEE Trans. Autom. Control*, vol. 50, no. 2, pp. 245–249, Feb. 2005.
- K. A. Bordignon and W. C. Durham, "Closed-form solutions to constrained control allocation problem," *J. Guid., Control, Dyn.*, vol. 18, no. 5, pp. 1000–1007, Sep. 1995.
- J. A. M. Petersen and M. Bodson, "Constrained quadratic programming techniques for control allocation," *IEEE Trans. Control Syst. Technol.*, vol. 14, no. 1, pp. 91–98, Jan. 2006.
- L. Zaccarian, "Dynamic allocation for input redundant control systems," *Automatica*, vol. 45, no. 6, pp. 1431–1438, Jun. 2009.
- M. Kirchengast, M. Steinberger, and M. Horn, "Input matrix factorizations for constrained control allocation," *IEEE Trans. Autom. Control*, vol. 63, no. 4, pp. 1163–1170, Apr. 2018.
- X. Zhao, Q. Zong, B. Tian, D. Wang, and M. You, "Finite-time fault-tolerant formation control for multiquadrotor systems with actuator fault," *Int. J. Robust Nonlinear Control*, vol. 28, no. 17, pp. 5386–5405, Nov. 2018.
- Z. Zheng, M. Qian, P. Li, and H. Yi, "Distributed adaptive control for UAV formation with input saturation and actuator fault," *IEEE Access*, vol. 7, pp. 144638–144647, 2019.
- X. Yang, Y. Wang, J. Yang, and T. Wang, "Fault-tolerant control based on fixed-time observer for a 3-DOF helicopter system," *Int. J. Control, Autom. Syst.*, vol. 18, no. 5, pp. 1–8, Jun. 2020.
- D. Bozorgnia and A. K. Sedigh, "A new control allocation methodology based on the pseudo inverse along the null space," in *Proc. 21st Iranian Conf. Electr. Eng. (ICEE)*, Mashhad, Iran, May 2013, pp. 1–4.
- T. Peni, B. Vanek, G. Liptak, Z. Szabo, and J. Bokor, "Nullspace-based input reconfiguration architecture for overactuated aerial vehicles," *IEEE Trans. Control Syst. Technol.*, vol. 26, no. 5, pp. 1826–1833, Sep. 2018.
- G.-X. Du, Q. Quan, and K.-Y. Cai, "Controllability analysis and degraded control for a class of hexacopters subject to rotor failures," *J. Intell. Robot. Syst.*, vol. 78, no. 1, pp. 143–157, Sep. 2014.
- G. X. Du, Q. Quan, B. X. Yang, and K. Y. Cai, "Controllability analysis for multirotor helicopter rotor degradation and failure," *J. Guid., Control, Dyn.*, vol. 38, no. 5, pp. 978–985, May 2015.
- Q. Quan, "Modeling and evaluation of propulsion system," in *Introduction to Multicopter Design and Control*, 2nd ed. Singapore: Springer, 2017, pp. 141–169.

- [41] S. Gao, C. D. Franco, D. Carter, D. Quinn, and N. Bezzo, "Exploiting ground and ceiling effects on autonomous UAV motion planning," in *Proc. Int. Conf. Unmanned Aircr. Syst. (ICUAS)*, Atlanta, GA, USA, Jun. 2019, pp. 768–777.
- [42] B. Kutz, U. Kowarsch, M. Kessler, and E. Kraemer, "Numerical investigation of helicopter rotors in ground effect," in *Proc. 30th AIAA Appl. Aerodynamics Conf.*, New Orleans, LA, USA, Jun. 2012, pp. 1–14.
- [43] S. T. Wu, "Servo and Servo control loop," in *Flight Control System*, 4th ed. Beijing, China: Beijing Univ. Aeronaut. Astronaut. Press, 2013, pp. 177–205.



**YIFAN XU** received the B.S. degree from the School of Instrumentation and Optoelectronic Engineering, Beihang University, in 2017. He is currently pursuing the Ph.D. degree with the School of Instrumentation and Optoelectronic Engineering. His main research interests are visual navigation, flight control, and autonomous landing.



**QIAN ZHANG** received the B.S. and Ph.D. degrees from the School of Instrumentation and Optoelectronic Engineering, Beihang University, in 2012 and 2019, respectively.

He is currently holding a postdoctoral position with the School of Aeronautic Science and Engineering, Beihang University. His current research interests include inertial navigation, unmanned aerial vehicle design, control and integrated navigation, as well as fault detection and diagnosis.



**ZELONG YU** received the B.S. degree from the School of Instrumentation and Optoelectronic Engineering, Beihang University, in 2016, where he is currently pursuing the Ph.D. degree with the School of Instrumentation and Optoelectronic Engineering. His main research interests are flight dynamics, flight control, and UAV navigation.

...